






Cryogenic origin of fractionation between perchlorate and chloride under modern martian climate

Dongdong Li ^{1,2}, Yu-Yan Sara Zhao ^{3,4,5✉}, Pierre-Yves Meslin ⁶, Margaux Vals ⁷, François Forget ⁷ & Zhongchen Wu⁸

The high perchlorate (ClO_4^-) to chloride (Cl^-) ratios observed at the Phoenix landing site, northern polar region of Mars, have been puzzling since detection. However, a lack of understanding of perchlorate-chloride-water systems under cryogenic conditions makes it difficult to assess $\text{ClO}_4^-/\text{Cl}^-$ ratios during deliquescence-related processes. Here we quantitatively evaluate $\text{ClO}_4^-/\text{Cl}^-$ fractionation in deliquescence-induced brines of magnesium- and calcium-perchlorate-chloride salt mixtures under subzero conditions, by measuring solubility data and constructing temperature-dependent thermodynamic models. We find that under specific relative humidity (RH) and temperature (T) conditions, deliquescence of perchlorate-chloride mixtures may form brines with fractionated $\text{ClO}_4^-/\text{Cl}^-$ signatures. Appropriate RH- T , water-limited conditions, and aeolian processes are required to produce and preserve the elevated $\text{ClO}_4^-/\text{Cl}^-$ signatures in soils. Under the present climate, the north polar region can support $\text{ClO}_4^-/\text{Cl}^-$ fractionation and potentially enrich perchlorate for longer periods on global Mars. This highlights the uniqueness of Mars' arctic environment and its implications for modern habitability.

¹Key Laboratory of Comprehensive and Highly Efficient Utilization of Salt Lake Resources, Qinghai Institute of Salt Lakes, Chinese Academy of Sciences, Xining, China. ²Key Laboratory of Salt Lake Resources Chemistry of Qinghai Province, Xining, China. ³Center for Lunar and Planetary Sciences, Institute of Geochemistry, Chinese Academy of Sciences, Guiyang, China. ⁴CAS Center for Excellence in Comparative Planetology, Hefei, China. ⁵International Center for Planetary Science, College of Geosciences, Chengdu University of Technology, Chengdu, China. ⁶Institut de Recherche en Astrophysique et Planétologie (IRAP), Université de Toulouse, OMP-CNRS-UPS, Toulouse, France. ⁷Laboratoire de Météorologie Dynamique (LMD/IPSL/CNRS), Sorbonne Université, Paris, France. ⁸Institute of Space Sciences, Shandong University, Weihai, China. ✉email: zhaoyuyan@mail.gyig.ac.cn

Perchlorate (ClO_4^-) and chlorate (ClO_3^-) have important implications for the habitability of Mars, such as aqueous activities^{1–3}, redox capabilities^{4–6}, and bioavailability⁷. Understanding the distribution and speciation of oxychlorine species on Mars is also critical for understanding the chlorine cycle on the Martian soil-atmosphere interface⁸, and critical for the detection of organic signals, and hazards and in situ resources for future human exploration⁹. To date, perchlorate or oxychlorine species (ClO_x^- ; equivalent to $\text{ClO}_4^- + \text{ClO}_3^-$) have been detected on Mars in surface soils, sedimentary rocks, and Martian meteorites^{10–16}. Natural perchlorate and chlorate are also observed in (hyper)arid environments on Earth (e.g., Atacama, Antarctic Dry Valleys) and in the surface samples of the moon and chondritic meteorites, indicating a ubiquitous presence of oxychlorine species across the inner solar system^{17,18}.

Among all the sites where perchlorate has been reported on Mars, the Phoenix landing site (68.2188°N, 125.7492°W) of the Vastitas Borealis is unique. The surface soil samples exhibit high ClO_4^- abundance (0.62–0.67 wt%) and low Cl^- abundance (0.03–0.05 wt%)¹⁵, which results in an average $\text{ClO}_4^-/\text{Cl}^-$ molar ratio of 6.13. Assuming $\text{Cl}_{\text{total}} = \text{Cl}^- + \text{ClO}_4^-$, the average $\text{ClO}_4^-/\text{Cl}_{\text{total}}$ molar ratio is equivalent to a $\text{ClO}_4^-/\text{Cl}_{\text{total}}$ molar ratio of 0.85. For comparison, such high $\text{ClO}_4^-/\text{Cl}_{\text{total}}$ molar ratios are rare and distinctive from any other Mars or terrestrial natural samples analyzed to date. Two aeolian samples at Gale Crater (4.5895°S, 137.4417°E) contain comparable levels of ClO_x^- (0.38 ± 0.16 wt% for Rocknest; 0.21 ± 0.06 wt% for Gobabeb) but much lower $\text{ClO}_x^-/\text{Cl}_{\text{total}}$ ratios (0.20 ± 0.07 for Rocknest; 0.15 ± 0.04 for Gobabeb¹⁵). Perchlorate (≤ 0.1 wt%) has also been suggested for soils at the two Viking landing sites (Viking 1: 22.27°N, 312.05°E; Viking 2: 47.64°N, 225.71°W)¹⁹. Using the average Cl_{total} of 0.8 wt%²⁰ for calculation, the $\text{ClO}_4^-/\text{Cl}_{\text{total}}$ ratio is estimated to be 0.04. Sedimentary outcrops of Gale Crater show a large variation in ClO_x^- abundances (from ~0 to 1.2 wt%), and the $\text{ClO}_x^-/\text{Cl}_{\text{total}}$ molar ratios are generally between 0.04 ± 0.02 and 0.18 ± 0.04, with only one exception of 0.27 ± 0.10 (mudstone sample “Cumberland”)¹⁵. Martian meteorites “EETA79001” (0.00006 wt% ClO_4^- ; 0.00014 wt% ClO_3^-)¹⁴ and “Tissint” (0.00007 wt% ClO_4^-)¹⁶ report $\text{ClO}_x^-/\text{Cl}_{\text{total}}$ ratios of 0.20 and 0.001, respectively. Of the terrestrial soils/caliches explored to date, Atacama samples contain the highest $\text{ClO}_4^-/\text{Cl}_{\text{total}}$ molar ratio of 0.0008¹⁷. Other terrestrial and extraterrestrial soil/rock samples have $\text{ClO}_4^-/\text{Cl}_{\text{total}}$ molar ratios at least an order of magnitude lower than those of Atacama samples^{17,18}.

High $\text{ClO}_4^-/\text{Cl}^-$ and $\text{ClO}_4^-/\text{Cl}_{\text{total}}$ ratios found in Phoenix soils might be formed primarily via direct production of ClO_4^- from Cl^- (i.e., generation mechanisms) or some concentration pathways of already formed ClO_4^- (i.e., enrichment mechanisms). However, the generation mechanisms are unlikely because Martian and terrestrial natural samples rarely contain $\text{ClO}_4^-/\text{Cl}_{\text{total}}$ molar ratios higher than 0.2, and simulation experiments producing ClO_x^- species from chloride (via photochemistry, electrochemistry, and ozone oxidation) have not reported any $\text{ClO}_4^-/\text{Cl}_{\text{total}}$ molar ratios higher than 0.1^{21–24}. Enrichment mechanisms such as deliquescence of perchlorate salts (i.e., moisture-absorption and dissolution of the salts and eutectic melting of salt-ice mixtures) have been proposed to produce brines that may translocate and concentrate perchlorate^{1,25–27}. However, a lack of understanding of perchlorate-chloride-water ternary systems under cryogenic conditions makes it difficult to evaluate the $\text{ClO}_4^-/\text{Cl}^-$ signatures in such brines.

Here we quantitatively evaluate $\text{ClO}_4^-/\text{Cl}^-$ fractionation in deliquescence-induced brines of magnesium- and calcium-perchlorate-chloride salt mixtures under subzero conditions, by measuring solubility data (233.15 K to 273.15 K) and constructed phase diagrams (180 K to 300 K) with the aid of temperature-

dependent thermodynamic models. We find that under specific relative humidity (RH) and temperature (T) conditions, deliquescence of perchlorate-chloride mixtures may form brines with fractionated $\text{ClO}_4^-/\text{Cl}^-$ signatures. Appropriate RH- T , water-limited conditions, and aeolian processes are required to produce and preserve the elevated $\text{ClO}_4^-/\text{Cl}^-$ signatures in soils. Under the present climate, the north polar region can support $\text{ClO}_4^-/\text{Cl}^-$ fractionation and potentially enrich perchlorate for longer periods on global Mars. Our work highlights that the high $\text{ClO}_4^-/\text{Cl}^-$ ratios detected in the Phoenix surface soil are produced by local environmental conditions and surface processes and may not be generalized to global Mars. It also indicates the uniqueness of Mars' arctic environment and its implications for modern habitability. In addition, the high $\text{ClO}_4^-/\text{Cl}^-$ signatures might be further used as a chemical signature to infer deliquescence in a liquid water-limited environment for Mars.

Results and discussion

Thermodynamic constraints on deliquescence of perchlorate-chloride-water systems. We focus on the ternary systems $\text{Mg}(\text{ClO}_4)_2 + \text{MgCl}_2 + \text{H}_2\text{O}$ and $\text{Ca}(\text{ClO}_4)_2 + \text{CaCl}_2 + \text{H}_2\text{O}$, which are the two most plausible systems suggested for soluble salts in Phoenix soils^{28–30}. Using isothermal solid-liquid equilibrium experiments, we experimentally measure solubility data at 273.15 K, 248.15 K, and 233.15 K for the $\text{Mg}(\text{ClO}_4)_2 + \text{MgCl}_2 + \text{H}_2\text{O}$ system (Supplementary Table 1) and at 263.15 K, 248.15 K, and 233.15 K for the $\text{Ca}(\text{ClO}_4)_2 + \text{CaCl}_2 + \text{H}_2\text{O}$ system (Supplementary Table 2), respectively. Supported by these ternary solubility data, we developed reliable temperature-dependent thermodynamic models for these ternary systems from 180 K to 300 K. The experimental and modeling results and validation of the thermodynamic models are available in the Supplementary Information (Supplementary Notes 1–5; Supplementary Tables 3–6; Supplementary Figs. 4–15).

During deliquescence of perchlorate-chloride salt mixtures, the substantial difference in solubility of perchlorate- and chloride- salts under specific RH- T conditions may result in fractionated $\text{ClO}_4^-/\text{Cl}^-$ signatures in the formed brines. Deliquescence surfaces of Mg- and Ca- perchlorate-chloride salt mixtures (i.e., $\text{Mg}(\text{ClO}_4)_2 \cdot 6\text{H}_2\text{O} + \text{MgCl}_2 \cdot x\text{H}_2\text{O}$, $x = 6, 8, 12$; $\text{Ca}(\text{ClO}_4)_2 \cdot 6\text{H}_2\text{O} + \text{CaCl}_2 \cdot 6\text{H}_2\text{O}$) in the coordinates of $\text{ClO}_4^-/\text{Cl}_{\text{total}}$ -RH- T are shown in Fig. 1 (Supplementary Data 1). For a specific salt mixture, the intersections of the deliquescence surface and the lower- and upper- T boundaries (i.e., dark cyan and dark red planes, respectively, in Fig. 1) constrain the RH- T conditions allowing for $\text{ClO}_4^-/\text{Cl}^-$ fractionation to occur. Deliquescence of perchlorate salt is preferred between the two boundaries while partial chloride salt remains solid, producing a brine with elevated $\text{ClO}_4^-/\text{Cl}^-$ ratios compared to its parent salt mixture. Above the upper T boundary, both perchlorate and chloride salts can fully deliquesce; under the lower T boundary, both perchlorate and chloride salts remain solids. Neither of the latter two cases would produce fractionated $\text{ClO}_4^-/\text{Cl}^-$ signatures.

Note that we did not include chlorate (ClO_3^-) in our experiments and model, although it is an essential component of oxychlorine species that may be present at both Phoenix site³⁰ and Gale Crater^{9,31} on Mars, with equal or higher abundances than perchlorates²⁴. The rationales for not involving chlorate in this work are mainly because (i) general lack of water activity, thermal and cryogenic solubility data for binary chlorate systems; (ii) the absence of ternary solubility data on chlorate systems; and (iii) experimental complexities to include Cl^- , ClO_4^- and ClO_3^- in one system. Consequently, the subsequent discussion and conceptual model in the following sections are limited to the $\text{ClO}_4^-/\text{Cl}^-/\text{H}_2\text{O}$ system without considering the potential interference of chlorate. Future systematic experimental and

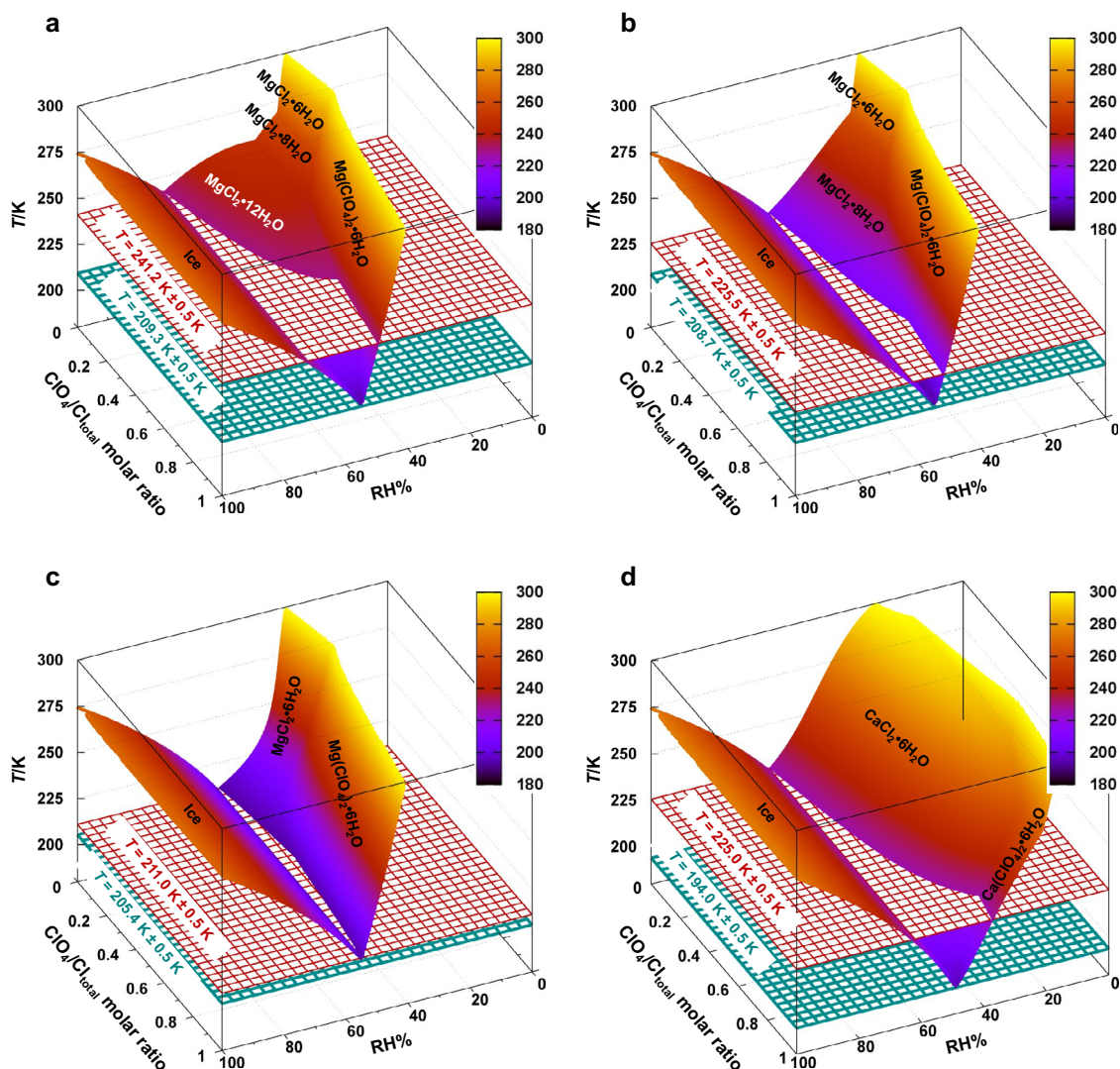


Fig. 1 Deliquescence surfaces of mixed hydrated Mg- and Ca-perchlorate/chloride salt mixtures calculated using thermodynamic models. **a–c** show the ternary system $\text{Mg}(\text{ClO}_4)_2 + \text{MgCl}_2 + \text{H}_2\text{O}$ with the lowest eutectic of thermodynamically stable state (**a**: $\text{Mg}(\text{ClO}_4)_2 \cdot 6\text{H}_2\text{O} + \text{MgCl}_2 \cdot 12\text{H}_2\text{O} + \text{ice}$) and metastable state (**b**: $\text{Mg}(\text{ClO}_4)_2 \cdot 6\text{H}_2\text{O} + \text{MgCl}_2 \cdot 8\text{H}_2\text{O} + \text{ice}$; **c**: $\text{Mg}(\text{ClO}_4)_2 \cdot 6\text{H}_2\text{O} + \text{MgCl}_2 \cdot 6\text{H}_2\text{O} + \text{ice}$). **d** shows the ternary system $\text{Ca}(\text{ClO}_4)_2 + \text{CaCl}_2 + \text{H}_2\text{O}$ under a thermodynamically stable state with the lowest eutectic of $\text{Ca}(\text{ClO}_4)_2 \cdot 6\text{H}_2\text{O} + \text{CaCl}_2 \cdot 6\text{H}_2\text{O} + \text{ice}$. Colored deliquescence surfaces represented by the legend are the interfaces for the phase transition of ternary $\text{ClO}_4^-/\text{Cl}^-/\text{H}_2\text{O}$ systems in each salt mixture. The dark cyan planes and dark red planes are the lower- and upper- T boundaries between which $\text{ClO}_4^-/\text{Cl}^-$ fractionation can occur. The lower- T boundary plane intercepts the minima of the ternary deliquescence surfaces, below which no deliquescence would occur. The upper- T boundary plane intercepts the minima of the binary deliquescence surfaces of the chloride-water system (i.e., $\text{ClO}_4^-/\text{Cl}^-$ molar ratio = 0), above which both ClO_4^- and Cl^- can be completely dissolved and no $\text{ClO}_4^-/\text{Cl}^-$ fractionation would occur.

modeling work on binary and ternary chlorate systems for cryogenic conditions is necessary to obtain fundamental insights.

Deliquescence and potential perchlorate/chloride fractionation at the Phoenix site versus Gale Crater. Combining the thermodynamic constraints and in situ RH- T measurements, we can further constrain the deliquescence behavior of Mg- and Ca-perchlorate-chloride salt mixtures at the Phoenix site and Gale Crater on Mars. At the Phoenix site, the surface RH- T conditions recorded by the Thermal and Electrical Conductivity Probe (TECP; recalibrated data)³² can support the deliquescence of Mg- and Ca-perchlorate-chloride salt mixtures (Fig. 2a; Supplementary Data 2). Of the four salt mixtures, the RH- T data of the Phoenix site overlap well with the RH- T condition ranges supporting the $\text{ClO}_4^-/\text{Cl}^-$ fractionation (i.e., intersections of the deliquescence surfaces and the lower-

and upper- T boundaries) for $\text{Mg}(\text{ClO}_4)_2 \cdot 6\text{H}_2\text{O}$ - $\text{MgCl}_2 \cdot 6\text{H}_2\text{O}$ (Fig. 2a-III) and $\text{Ca}(\text{ClO}_4)_2 \cdot 6\text{H}_2\text{O}$ - $\text{CaCl}_2 \cdot 6\text{H}_2\text{O}$ (Fig. 2a-IV), which may facilitate the formation of brines with elevated $\text{ClO}_4^-/\text{Cl}^-$ signatures. The RH- T data are close but not in contact with the lowest eutectic points for the $\text{Mg}(\text{ClO}_4)_2 \cdot 6\text{H}_2\text{O}$ - $\text{MgCl}_2 \cdot 12\text{H}_2\text{O}$ or $\text{Mg}(\text{ClO}_4)_2 \cdot 6\text{H}_2\text{O}$ - $\text{MgCl}_2 \cdot 8\text{H}_2\text{O}$ cases (Fig. 2a-I and 2a-II). However, given the limited duration of the Phoenix mission (total lifetime 152 sols; $L_s = 77^\circ$ to $L_s = 151^\circ$)³³, we speculate that the RH- T conditions of Phoenix also likely support at least partial deliquescence and $\text{ClO}_4^-/\text{Cl}^-$ fractionation in the latter cases.

At Gale Crater, the Rover Environmental Monitoring Station (REMS) onboard the Curiosity rover recorded RH- T data. We examined the in situ RH- T data of the first four Martian years (Figure S17), which account for all the available data at the time of writing. Since the REMS data record the RH- T conditions at 1.6 m above the ground, surface brightness temperatures (T_{surf})

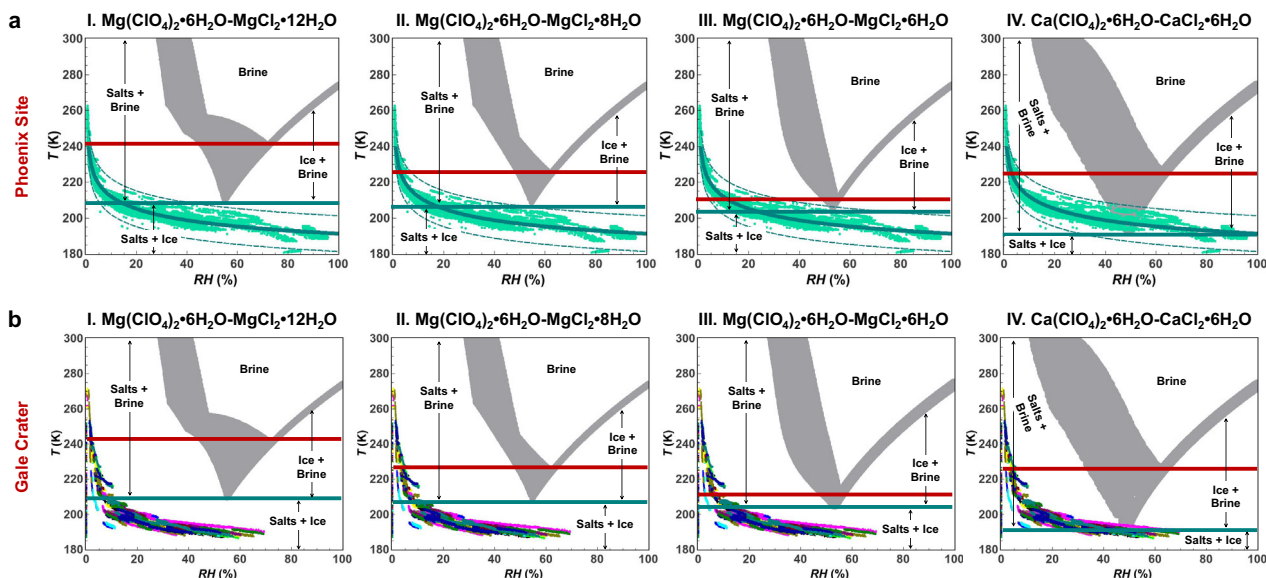


Fig. 2 Deliquescence-induced brine formation at the Phoenix landing site and Gale Crater. **a** In situ RH-*T* data of the Phoenix landing site are overlaid onto the deliquescence surfaces of the salt mixtures. I: $\text{Mg}(\text{ClO}_4)_2 \cdot 6\text{H}_2\text{O} + \text{MgCl}_2 \cdot 12\text{H}_2\text{O}$; II: $\text{Mg}(\text{ClO}_4)_2 \cdot 6\text{H}_2\text{O} + \text{MgCl}_2 \cdot 8\text{H}_2\text{O}$; III: $\text{Mg}(\text{ClO}_4)_2 \cdot 6\text{H}_2\text{O} + \text{MgCl}_2 \cdot 6\text{H}_2\text{O}$; and IV: $\text{Ca}(\text{ClO}_4)_2 \cdot 6\text{H}_2\text{O} + \text{CaCl}_2 \cdot 6\text{H}_2\text{O}$. The dark gray regions are the projection of the ternary deliquescence surfaces, and the dark cyan and dark red horizontal lines are the projections of the lower- and upper- *T* boundary planes, respectively, as shown in Fig. 1. The green dots are in situ RH-*T* measurements. The thick solid dark-cyan curve is the best fit line, and the thin dashed dark-cyan curves are the 10 K uncertainty boundaries. Salt mixtures of $\text{Mg}(\text{ClO}_4)_2 \cdot 6\text{H}_2\text{O} - \text{MgCl}_2 \cdot 6\text{H}_2\text{O}$ and $\text{Ca}(\text{ClO}_4)_2 \cdot 6\text{H}_2\text{O} - \text{CaCl}_2 \cdot 6\text{H}_2\text{O}$ may facilitate the formation of brines with elevated $\text{ClO}_4^-/\text{Cl}^-$ signatures. **b** In situ RH-*T* data of Gale Crater overlaid on the deliquescence surfaces of the salt mixtures. The dark gray ternary deliquescence surfaces and the lower- and upper- *T* boundary lines of subfigures I to IV are the same as shown in (a). The colored dots are the in situ RH-*T* data (REMS; sols 526, 531, 548, 549, 551, and 554 to 561 with maximum yearly humidity). The RH-*T* conditions of the first Martian year at Gale Crater would support the deliquescence of $\text{Ca}(\text{ClO}_4)_2 \cdot 6\text{H}_2\text{O} - \text{CaCl}_2 \cdot 6\text{H}_2\text{O}$ but not for any of the Mg salt mixtures.

measured by the Ground Temperature Sensor (GTS) were also processed for comparison. We find that the REMS and GTS datasets show no difference in terms of supporting deliquescence at Gale Crater, but the GTS data contain higher uncertainties that would propagate to the derived RH data (Supplementary Figs. 18 and 19). Therefore, we use the REMS data to discuss the Gale Crater environments (Fig. 2b). The variation in RH-*T* conditions along the traverse of the Curiosity rover is primarily due to the change in ground properties (e.g., thermal inertia and porosity) from loosened regolith to solid bedrock, as the rover started to climb the Mount Sharp (sol 1800 onwards)³⁴. Consequently, the RH-*T* conditions of the first three Martian years at Gale Crater would support the deliquescence of $\text{Ca}(\text{ClO}_4)_2 \cdot 6\text{H}_2\text{O} - \text{CaCl}_2 \cdot 6\text{H}_2\text{O}$ but not for any of the Mg salt mixtures (Fig. 2b; Supplementary Fig. 17). In the fourth Martian year, deliquescence and $\text{ClO}_4^-/\text{Cl}^-$ fractionation can occur for both the $\text{Mg}(\text{ClO}_4)_2 \cdot 6\text{H}_2\text{O} - \text{MgCl}_2 \cdot 6\text{H}_2\text{O}$ and $\text{Ca}(\text{ClO}_4)_2 \cdot 6\text{H}_2\text{O} - \text{CaCl}_2 \cdot 6\text{H}_2\text{O}$ systems (Supplementary Fig. 17). The O_2 and HCl evolution patterns during pyrolysis of the aeolian samples “Rocknest” and “Gobabeb” suggest that the cations of the oxychlorine species are likely Na, K and Ca⁹. We find that the absence of $\text{ClO}_4^-/\text{Cl}^-$ fractionation in these samples during the first three Martian years might further rule out Ca-perchlorate. The lack of pyrolysis analyses for oxychlorine in soil/aeolian samples after “Gobabeb” (elevation –4.424 km)⁹ makes it difficult to evaluate the possible $\text{ClO}_4^-/\text{Cl}^-$ molar ratios at higher elevations along the rover traverse. Note that $\text{ClO}_4^-/\text{Cl}^-$ ratios detected in the drilled samples from the bedrock mainly represent rock characteristics influenced by aqueous processes rather than atmosphere–solid interactions and thus are irrelevant to the model we discuss in this study.

Deliquescent brine at the Phoenix site would contain substantially elevated $\text{ClO}_4^-/\text{Cl}^-$ signatures compared to their

parent salt mixtures. For example, the deliquescence of the $\text{Mg}(\text{ClO}_4)_2 \cdot 6\text{H}_2\text{O} - \text{MgCl}_2 \cdot 6\text{H}_2\text{O}$ salt mixture would produce a brine with a nearly fixed $\text{ClO}_4^-/\text{Cl}^-$ molar ratio of 2.5 (Fig. 3a; Supplementary Data 3). The $\text{Ca}(\text{ClO}_4)_2 \cdot 6\text{H}_2\text{O} - \text{CaCl}_2 \cdot 6\text{H}_2\text{O}$ salt mixture would form a brine with a $\text{ClO}_4^-/\text{Cl}^-$ molar ratio ranging from 9.0 to 13.3 (Fig. 3b). For $\text{MgCl}_2 \cdot 8\text{H}_2\text{O}$ and $\text{MgCl}_2 \cdot 12\text{H}_2\text{O}$ instead of $\text{MgCl}_2 \cdot 6\text{H}_2\text{O}$, using the inferred lowest eutectic points for calculation, the formed brines would have $\text{ClO}_4^-/\text{Cl}^-$ molar ratios of 14.4 and 62.6, respectively. Our calculations assume complete separation of formed brines and residual chloride salts and thus provide the upper limit for the deliquescence-induced $\text{ClO}_4^-/\text{Cl}^-$ molar ratios. The measured $\text{ClO}_4^-/\text{Cl}^-$ of 6.13¹⁵ in Phoenix soil can form via either Mg or Ca salt mixtures, but the $\text{Mg}(\text{ClO}_4)_2 \cdot 6\text{H}_2\text{O} - \text{MgCl}_2 \cdot 6\text{H}_2\text{O}$ system is unlikely to be the parent salt mixture since it cannot produce a $\text{ClO}_4^-/\text{Cl}^-$ ratio higher than 2.5.

For reference, we also analyzed relevant data from McMurdo Dry Valleys (MDV), Antarctica. The MDV is considered an excellent analog site for the northern plains of Mars because of the arid conditions, intense UV solar radiation, diurnal freeze/thaw cycles, sparse snowfall, cryogenic processes, low mean temperatures, and Mars-like surface topography³⁵. Our results show that the RH-*T* conditions of Antarctica would produce substantial liquid water and dissolve both ClO_4^- and Cl^- and may not result in $\text{ClO}_4^-/\text{Cl}^-$ fractionation (Supplementary Note 6 and Supplementary Fig. 20). This result is consistent with the absence of $\text{ClO}_4^-/\text{Cl}^-$ fractionation found in samples of MDV^{35,36}.

RH-*T* conditions of global Mars that can support perchlorate/chloride fractionation. Using the RH-*T* constraints obtained from the phase diagrams (Supplementary Fig. 21; Supplementary Table 7), we map the Martian surface for regions of which the RH-

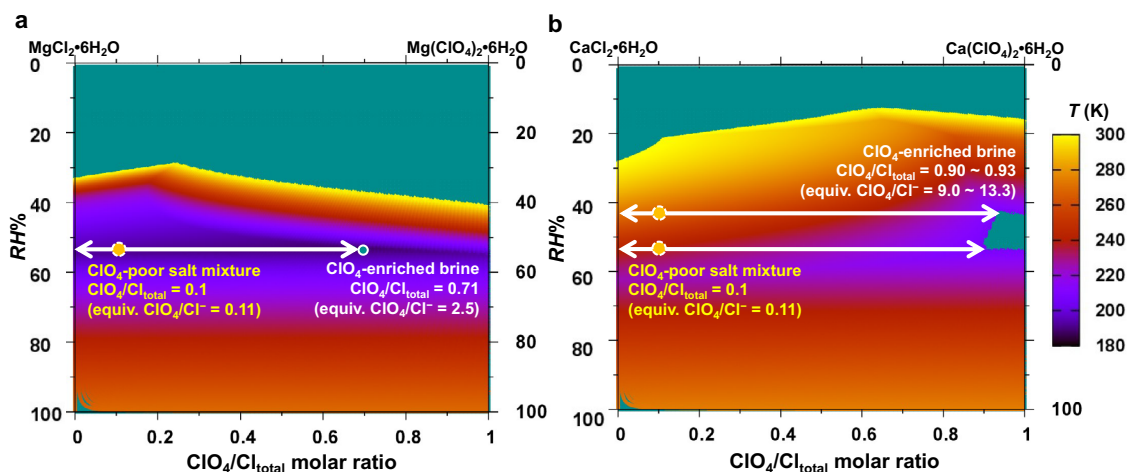


Fig. 3 Deliquescence-induced $\text{ClO}_4^-/\text{Cl}^-$ fractionation at the Phoenix landing site with $\text{Mg}(\text{ClO}_4)_2 \cdot 6\text{H}_2\text{O} + \text{MgCl}_2 \cdot 6\text{H}_2\text{O}$ and $\text{Ca}(\text{ClO}_4)_2 \cdot 6\text{H}_2\text{O} + \text{CaCl}_2 \cdot 6\text{H}_2\text{O}$ salt mixtures. **a** For the $\text{Mg}(\text{ClO}_4)_2 \cdot 6\text{H}_2\text{O} + \text{MgCl}_2 \cdot 6\text{H}_2\text{O}$ salt mixture, the deliquescence surface (i.e., color surface represented by the legend) intersect with the RH- T conditions (i.e., cyan surface: the best fit line of the scattered RH- T data in situ determined by Phoenix lander and independent of $\text{ClO}_4^-/\text{Cl}_{\text{total}}$) in a very small region (i.e., the cyan dot), with a $\text{ClO}_4^-/\text{Cl}^-$ molar ratio of 2.5. The RH is calculated based on $\text{RH}\% = 100 \cdot a_w$ by the thermodynamic model. **b** For the $\text{Ca}(\text{ClO}_4)_2 \cdot 6\text{H}_2\text{O} + \text{CaCl}_2 \cdot 6\text{H}_2\text{O}$ salt mixture, the deliquescence surface (i.e., color surface represented by the legend) intersect with the RH- T conditions (cyan surface) in a relatively large region (i.e., cyan trapezoid), with $\text{ClO}_4^-/\text{Cl}^-$ molar ratios ranging from 9.0 to 13.3. Starting with Mg- and Ca- salt mixtures that are initially poor in perchlorate (e.g., yellow dots as $\text{ClO}_4^-/\text{Cl}^-$ molar ratio = 0.11), deliquescence would simultaneously produce a nearly pure chloride salt (on the left arrow) and a ClO_4^- -rich brine (on the right arrow to the dark cyan intersection). The maximum $\text{ClO}_4^-/\text{Cl}^-$ molar ratios of deliquescence-induced brine are determined by the types of parent salt mixtures, regardless of the initial $\text{ClO}_4^-/\text{Cl}^-$ ratios in the salt mixtures. See Supplementary Fig. 16 for additional discussion on the ternary phase diagram and the projections.

T conditions can support $\text{ClO}_4^-/\text{Cl}^-$ fractionation throughout a Mars year under present climatic conditions (Fig. 4; Supplementary Data 4). Note that the data used for mapping are numerical simulation outputs of the LMD General Circulation Model, not measured climate data of Mars (see Methods section for details). The idiosyncrasies of the water cycle in the northern hemisphere and the parental salts are the main controlling factors. Globally, the north polar region can maintain $\text{ClO}_4^-/\text{Cl}^-$ fractionation for the longest time with both Mg- and Ca- salt mixtures, consistent with the high $\text{ClO}_4^-/\text{Cl}^-$ fractionation signatures detected at the Phoenix site. In contrast, the south polar region of Mars (60°S and higher latitude) is similar to the equatorial region and does not likely support $\text{ClO}_4^-/\text{Cl}^-$ fractionations.

In addition to the north polar region, the Acidalia-Chryse and Utopia regions also appear to be favorable, to a lesser extent, to $\text{ClO}_4^-/\text{Cl}^-$ fractionation, as well as a few large basins (e.g., Hellas Planitia and Argyre Planitia), where Ca-salt mixtures could fractionate. The positive topography (e.g., highlands, Olympus Mons), in turn, would not support $\text{ClO}_4^-/\text{Cl}^-$ fractionation even at locations within the mid-latitude regions.

Figure 4 shows that the Ca- salt mixture can result in deliquescence and the consequent $\text{ClO}_4^-/\text{Cl}^-$ fractionation for a longer time (maximum ~8% of a Mars year or ~50 sols per Mars year) and in a more extensive region including equatorial latitudes compared to the Mg- salt mixtures. However, we speculate that Ca-perchlorates-chlorides are unlikely to be the predominant salt phases on the Martian surface. Ca^{2+} release by the weathering of Martian basalts is lower than that of Mg^{2+} ³⁷ and Ca^{2+} tends to precipitate as sulfates rather than chlorides^{38–40}. The subsequent oxidation of chlorides (e.g., with cations Mg, Na, K) via photochemistry, electrochemistry, or ozone^{23–25,41} would likely produce perchlorates sharing the same cations as their parent chlorides.

A conceptual model for the formation and preservation of high perchlorate/chloride ratios on the Martian surface. Three

essential factors are crucial for the formation and preservation of fractionated $\text{ClO}_4^-/\text{Cl}^-$ signatures. First, the RH- T conditions should be suitable for deliquescence to occur. Second, the water source should be limited in quantity since any substantial liquid-water interactions would dissolve both ClO_4^- and Cl^- and obliterate the fractionation signatures. Third, subsequent separation of the perchlorate-enriched brines and chloride-enriched salts is necessary for the $\text{ClO}_4^-/\text{Cl}^-$ signatures to be detected. In this scenario, the transient brines formed under water-limited conditions would be primarily confined onto the particle surface or intergranular pores, and thus, their spatial translocation would be substantially constrained. We suggest that translocation of the salts with soil/dust particles via aeolian processes may be a more practical way to form a locally homogeneous $\text{ClO}_4^-/\text{Cl}^-$ signature, as detected in Phoenix soils.

We propose a conceptual model for forming and preserving high $\text{ClO}_4^-/\text{Cl}^-$ ratios on the present Martian surface (Fig. 5). (1) Aeolian processes (e.g., dust storms/dust devils) continuously transfer dust/soil particles coated with perchlorate-chloride salt mixtures ($\text{ClO}_4^-/\text{Cl}_{\text{total}}$ ratios presumably at the global-average level) to some region (e.g., the Mars arctic region). Dust is likely to be the primary carrier of perchlorates and chlorides⁴², given the high efficiency in converting chlorides to perchlorates on the dust particles^{23,24}. (2) Under appropriate RH- T conditions (e.g., the Phoenix landing site), deliquescence of the perchlorate-chloride salt mixture by interaction with water-vapor or water-ice produces transient brines containing fractionated $\text{ClO}_4^-/\text{Cl}^-$ signatures. The specific ratios depend on the parental salts and the RH- T conditions. (3) Dust/soil particles cemented with brines would be more resistant to aeolian translocation (e.g., during the impact of saltating particles) than dry ClO_4^- -depleted dust/soil particles. In this way, perchlorates preferentially accumulate while chlorides are more likely to be transported locally or regionally.

The texture of the Phoenix soils supports this conceptual model well—a geologically young soil (for the current RH- T conditions to remain applicable), with active reworking (by dust deposition/lifting) and without interaction with extensive liquid water. The

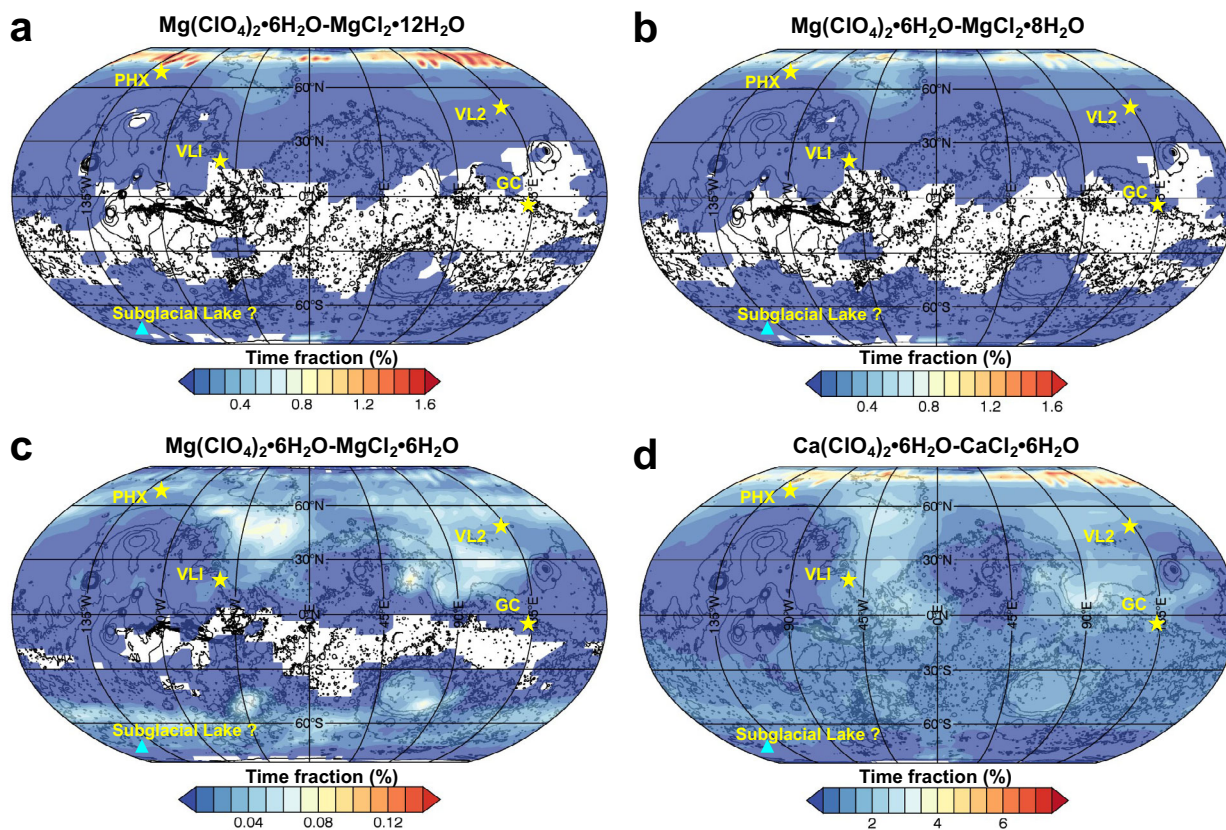


Fig. 4 Time fraction of a Mars year under the present climate where surface RH-T conditions can support $\text{ClO}_4^-/\text{Cl}^-$ fractionation for Mg- or Ca-perchlorate-chloride salt mixtures. **a–c** are for the Mg-salt mixture, with the hydrated state of Mg-chloride varying from $12\text{H}_2\text{O}$, $8\text{H}_2\text{O}$, and $6\text{H}_2\text{O}$, respectively. **d** is for $\text{Ca}(\text{ClO}_4)_2 \cdot 6\text{H}_2\text{O} - \text{CaCl}_2 \cdot 6\text{H}_2\text{O}$. A $\text{ClO}_4^-/\text{Cl}_{\text{total}}$ molar ratio >0.2 is used as the indicator of perchlorate/chloride fractionation and the corresponding boundary conditions for each salt mixture are shown in Supplementary Fig. 19 and Supplementary Table 7. PHX represents the Phoenix landing site; VLI and VL2 represent Viking Landers 1 and 2, respectively; GC represents the Gale Crater. Regions without colors indicate that the surface RH-T conditions would never support $\text{ClO}_4^-/\text{Cl}^-$ fractionation. Globally, the north polar region can maintain $\text{ClO}_4^-/\text{Cl}^-$ fractionation for the longest time with both Mg- and Ca- salt mixtures. Compared to the Phoenix site, Viking Landers 1 and 2 and Gale Crater are located in regions with a shorter time fraction. Dynamics of the water cycle and parental salts are critical controlling factors. See the text for discussion.

cohesive and cloddy nature of the soils indicates an interaction between ice/absorbed water and salty soil in place⁴³. The soil profile demonstrates homogeneity in terms of soil microstructure, and no substantial difference in soil particles is observed above and below the ice table⁴⁴. Microscopic analysis of the Phoenix soil particles suggests that the soil is aeolian in origin⁴⁵, and the particles may have undergone long-distance translocation (>500 km) via air-fall dust processes or saltation⁴⁶. The three soil samples “Rosy Red”, “Sorceress 1”, and “Sorceress 2”, composing the topmost ~ 5 cm of the soil profile, each contain evenly distributed ClO_4^- concentrations and high $\text{ClO}_4^-/\text{Cl}^-$ ratios.

As a result of strong winds induced by baroclinic transient waves occurring at high northern latitudes in the autumn and winter seasons, most regional-scale dust storms originate from the northern plains^{47–51}. Frequent local and regional-scale dust storms take place between latitudes ~ 30 – 80°N ⁴⁹. These dust storms enable regional or global circulation of dust across latitudes and facilitate material exchange in and out of the north polar region. Dust storm simulations (e.g., for MY25 and MY34) indicate the general north polar region and the Phoenix site to be an active region in terms of dust activity⁵⁰, which may facilitate dust/soil translocation in that region. Interestingly, the Acidalia-Chryse and Utopia Planitiae regions, which also stand out in Fig. 4, are known to be “storm tracks” where regional-scale dust storms develop⁵⁰, which acts in favor of the proposed scenario in these regions.

The essential factors required for the formation and preservation of fractionated $\text{ClO}_4^-/\text{Cl}^-$ signatures in turn impose environmental constraints on the site where high $\text{ClO}_4^-/\text{Cl}^-$ signatures are detected. At the Phoenix site, for instance, we estimated that the deposition of an ~ 5 -cm thick dust layer requires ~ 1.5 kyr to 13.7 kyr (Earth years) by using the rate of dust settling measured during the Phoenix mission lifetime (“fiducials” data of $0.05 \pm 0.04 \mu\text{m}$ per sol, representing any random patch on the lander deck⁵²). Additionally, by using the north polar dust sedimentation rates ($0.6\text{--}1 \text{ mg cm}^{-2} \text{ yr}^{-1}$)⁴⁹ and assuming a bulk density of 1.2 g cm^{-3} of the dust, we obtained a consistent estimated 6–10 kyr (Earth years) for a 5-cm dust accumulation. This estimated time-scale is consistent with the time proposed for ground ice formation by diffusive equilibrium (hundreds to thousands of years)⁵³ and the formation of a shallow ice table within ~ 100 kyr under the current Martian climate regime⁵⁴. Therefore, the active dust processes and the specific RH-T conditions may have lasted for approximately a few to tens of kyr at the Phoenix site.

Our study indicates that environmental conditions and surface processes operate cooperatively to produce and preserve fractionated $\text{ClO}_4^-/\text{Cl}^-$ signatures under the present climate of Mars. The north polar region of Mars, in particular, is a region that can best support $\text{ClO}_4^-/\text{Cl}^-$ fractionation and ClO_4^- enrichment. Such fractionation and enrichment of perchlorates, if lasting for a few tens to hundreds of kyr or longer, would support the

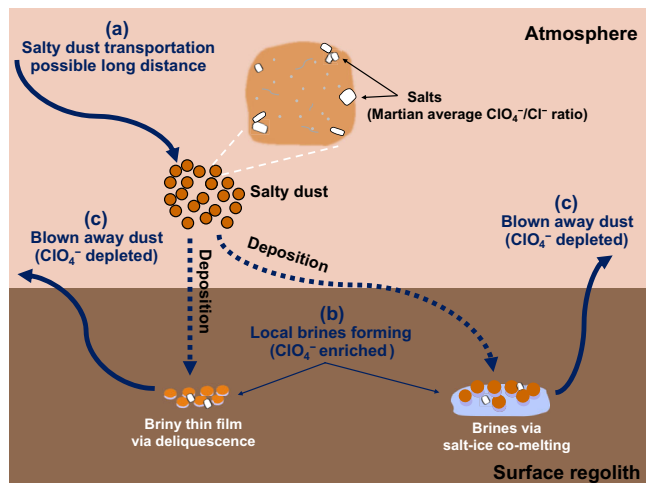


Fig. 5 A conceptual model for forming and preserving high perchlorate/chloride ratios on the present Martian surface by coupling briny-aeolian process. **a** Aeolian processes (e.g., dust storms/dust devils) continuously transfer dust/soil particles coated with perchlorate-chloride salt mixtures ($\text{ClO}_4^-/\text{Cl}_{\text{total}}$ ratios presumably at the global-average) in some regions (e.g., the Mars arctic region). **b** Under appropriate RH-T conditions, the deliquescence of the perchlorate-chloride salt mixture by interaction with water-vapor or water-ice can produce transient brines containing fractionated $\text{ClO}_4^-/\text{Cl}^-$ signatures. The specific ratios depend on the parent salts and the RH-T conditions. **c** Dust/soil particles cemented with brines would resist aeolian translocation better than dry ClO_4^- -depleted dust/soil particles. In this way, perchlorates preferentially accumulate in place while chlorides are more likely to be transported away.

formation of a lubricating brine in the basal ice layer and facilitate the flow of the northern ice cap³⁶. The enrichment of perchlorates in the north polar region also offers implications for modern habitability. On the one hand, the (meta)stable brines that were formed are likely high in salinity and low in water activity, which are not habitable to any known terrestrial life^{55,56}. On the other hand, concentrated perchlorates can facilitate water adsorption due to their hygroscopic characteristics and result in the regolith holding a substantial fraction of the water inventory⁵⁷. Such water-rich regolith may shelter against radiation doses and provide safe habitats underground for potential extant life⁵⁸.

Methods

Experimental measurements of ternary solubility at subzero temperatures.

An isothermal method was used to determine the solid-liquid phase equilibria in the ternary systems $\text{Mg}(\text{ClO}_4)_2 + \text{MgCl}_2 + \text{H}_2\text{O}$ and $\text{Ca}(\text{ClO}_4)_2 + \text{CaCl}_2 + \text{H}_2\text{O}$. The experiments were conducted at 273.15 K, 263.15 K, 248.15 K, and 233.15 K, respectively. Magnesium chloride hexahydrate and calcium chloride dihydrate ($\text{MgCl}_2 \cdot 6\text{H}_2\text{O}$, purity ≥ 98.0 wt%, CAS No. 7791-18-6; $\text{CaCl}_2 \cdot 2\text{H}_2\text{O}$, purity ≥ 99.0 wt%, CAS No. 10035-04-8; Shanghai Sinopharm Chemical Reagent Co., Ltd) were purified by one-time recrystallization with an approximately 60% salt recovery. The final purity, as analyzed by Inductively Coupled Plasma Emission Spectrometry was >99.95 wt%. Magnesium perchlorate hexahydrate ($\text{Mg}(\text{ClO}_4)_2 \cdot 6\text{H}_2\text{O}$, purity >99.99 wt% metals basis, CAS No. 13446-19-0, Aladdin Industrial Co.) and calcium perchlorate tetrahydrate ($\text{Ca}(\text{ClO}_4)_2 \cdot 4\text{H}_2\text{O}$, purity ≥ 99.8 wt%, CAS No. 15627-86-8, Acros) were directly used without further purification. Ultrapure water (18 M Ω) was used in all experiments.

A thermostatic water bath with a refrigerating machine (Lauda Command and DLK45, Germany) was used to perform the cryogenic phase equilibria experiments (Supplementary Fig. 1). The temperature uncertainty of the whole thermostat system was controlled within 0.05 K. A 250 mL flat-bottom glass tube with a PTFE stopper and overhead mechanical stirrer was used as the container (i.e., solubility cells in Supplementary Fig. 1). The reaction mixtures were prepared by weighing ultrapure water and the appropriate amount of perchlorate and chloride reagents to fill 1/4 of the reaction container. The container with the reaction mixture was lowered into a water bath until the water covered most of the container. The experiments were conducted at 273.15 K, 263.15 K, 248.15 K, and 233.15 K, respectively. The mixtures were equilibrated for five days at 273.15 K and for at

least ten days at 263.15 K, 248.15 K, and 233.15 K, due to the slow rates in reaching equilibrium at subzero temperatures. Throughout the experiments, the reaction mixtures were stirred thoroughly.

As a conventional analysis method used by physical chemists in thermodynamic experiments, the chemical compositions of the supernatants filtered using 0.45 μm syringe filters were determined by mass titration of Mg^{2+} , Ca^{2+} , and Cl^- , and subsequent subtraction of ClO_4^- according to charge balance. Cations Mg^{2+} and Ca^{2+} were titrated by EDTA solution calibrated using ZnO and CaCO_3 primary standards, respectively. Anion Cl^- was titrated by AgNO_3 solution calibrated using a NaCl primary standard. The relative uncertainties of the chemical analysis were within 0.3% for Mg^{2+} , Ca^{2+} and Cl^- , and 0.6% for ClO_4^- .

The chemical compositions of wet solids (i.e., directly scooped out of the reaction container without further processing) were also determined using the same analytical methods as for the supernatants. Solid phases in equilibrium with the solution at 273.15 K were identified using an X-ray diffractometer (XRD; X'Pert PRO, 2006 PANalytical with Cu K α radiation and $\lambda = 0.15406$ nm) at room temperature (Supplementary Fig. 2). For solid phases in equilibrium with the solution at temperatures lower than 273.15 K, Schreinemakers' wet residues method⁵⁹ was used instead of XRD analysis to avoid possible melting or decomposition of hydrated salts at room temperature. The Schreinemakers' wet residues method was a classical method in the phase diagram experimental determination for the salt-water system and its principle is illustrated in Supplementary Fig. 3. The overall relative uncertainties of the liquid and wet residual compositions in the experiments were within 2%. The details of the experimental methods and results are available in Supplementary Notes 1 and 2, respectively.

Thermodynamic modeling methods and results validation. The ISLEC software, i.e., Institute of Salt Lakes Equilibrium Calculator, was used in this study to model the solubility isotherms and generate the phase diagrams for the ternary $\text{Mg}(\text{ClO}_4)_2 + \text{MgCl}_2 + \text{H}_2\text{O}$ and $\text{Ca}(\text{ClO}_4)_2 + \text{CaCl}_2 + \text{H}_2\text{O}$ systems. The theoretical background, basic equations and implementation of the software can be found in a recent work⁶⁰. The software adopted a CALPHAD type (i.e., Computer Coupling of Phase Diagrams and Thermochemistry) thermodynamic framework and a Pitzer-Simonson-Clegg (PSC) excess Gibbs energy model to describe the non-ideality of the aqueous phase. Unlike the conventional solubility modeling method, the CALPHAD framework allowed the thermodynamic model for the aqueous system to be parameterized using various types of thermodynamic data, particularly the thermal data (e.g., enthalpy of dilution, enthalpy of solution, and heat capacity of aqueous solution and solids), to enhance the reliability of the temperature-dependent models. The PSC model was an advanced version of the classical Pitzer model updated by the Pitzer's group⁶¹. The ISLEC software used the Gibbs energy minimization (GEM) approach for solving the phase equilibria. The ISLEC software has successfully modeled extensive binary systems, ternary systems, and multicomponent systems down to ~ 200 K (see Code Statement for accessible link). A detailed description, parameters, and equations implemented by the ISLEC software for the studied ternary systems $\text{Mg}(\text{ClO}_4)_2 + \text{MgCl}_2 + \text{H}_2\text{O}$ and $\text{Ca}(\text{ClO}_4)_2 + \text{CaCl}_2 + \text{H}_2\text{O}$ are summarized in Supplementary Note 3. The experimental data collected from the literature for regressing the temperature-dependent binary perchlorate parameters are shown in Supplementary Table 3. All the thermodynamic parameters used are listed in Supplementary Tables 4 and 5. Details of validations of the modeling results are presented in Supplementary Notes 4 and 5.

Phase diagram calculation. Deliquescence occurs when the relative humidity (RH) in the gas-phase environment is at or above the mutual deliquescence relative humidity (MDRH) of a salt mixture. The MDRH data points therefore belong to the deliquescence surfaces of a salt mixture⁶². In a salt-solution model, RH can be derived using the water activity (a_w). At a given temperature, $\text{RH} = 100 \cdot a_w = 100 \cdot p_w/p_w^0$, where p_w and p_w^0 are the vapor pressure of the saturation solution and pure water, respectively. When a_w is of a solution in equilibrium with the salt, the calculated RH is MDRH. The a_w can be calculated using equation S16 in the Supplementary Information. The deliquescence surface data in an x -T-RH coordinate system were generated using the C codes (i.e., `islec_mars_mdrh_mg.c` and `islec_mars_mdrh_ca.c`; see Code Statement for accessible link). The x was calculated from the equilibrium molality of perchlorate and chloride in aqueous solution. These codes can be compiled using the GCC compiler on the Linux platform or the Dev-Cpp compiler on the Windows platform. The awk script can be used to format the output data produced by `islec_mars_mdrh_ca` for further visualization. These output data were then visualized with Gnuplot software for 2D and 3D plots. Detailed instructions can be found in the README file included in the source code package (link provided in Code Statement).

Mapping global Mars for the regional environments that may support $\text{ClO}_4^-/\text{Cl}^-$ fractionation. The regions that meet the $\text{RH-T}_{\text{surf}}$ requirements for $\text{ClO}_4^-/\text{Cl}^-$ fractionation, i.e., where environmental conditions overlap with the phase diagram of a specific salt mixture and can produce brine with $\text{ClO}_4^-/\text{Cl}_{\text{total}} > 0.2$ (Supplementary Fig. 17 and Supplementary Table 7), were mapped using the outputs of the

LMD General Circulation Model⁶³. It should be noted that the data used for plotting the map are numerical model outputs, not measured climate data of Mars.

The LMD GCM simulates water and dust transport, including the microphysics and radiative effects of water ice clouds, dust/ice sedimentation and condensation/sublimation of water/ice at the surface^{63–67}. The model has also been used to predict and analyze the night-time near-surface relative humidity on Mars⁶⁸. The model is continuously confronted with available observations to validate its results. Specifically, the LMD GCM model resolves the equations of the atmospheric circulation on a 3D global grid covering the Martian atmosphere and includes the main physical parametrizations responsible for the climatological forcing, such as radiative transfer, small-scale turbulence⁶³ or daytime thermal convection⁶⁹. Martian topography is based on MOLA (Mars Orbiter Laser Altimeter) data⁷⁰, whereas surface properties of the Martian soil (thermal inertia and albedo) were taken from TES observations⁷¹, except for the permanent ice of the North Pole, the main source of water released in the atmosphere, which is prescribed by the model⁶⁵. Radiative transfer takes into account the emission and absorption of CO₂ gas in infrared as well as the emission, absorption, and scattering of airborne dust⁶⁴ and water ice⁶⁶. The model simulates water and dust transport, including dust and ice sedimentation and condensation/sublimation of water ice at the surface^{63,67}. Water ice cloud microphysics have been introduced in the model to account for the interaction between dust and water condensing in the atmosphere⁶⁵, including the processes of nucleation, ice growth and scavenging, and thereby allowing the representation of supersaturation. Although the dust spatial distribution is explicitly predicted by the model, the dust column opacity is rescaled to match the observed opacities compiled as dust scenarios for each Martian year⁷² using a semi-interactive scheme developed⁷³. The simulation used for the mapping has been produced with the ‘climatology’ dust scenario, which is derived from the available observations of dust from multiple years without global planet-encircling dust storms and is therefore representative for a typical Martian year.

The grid resolution was set to a standard value of 5.625° × 3.75° longitude–latitude (64 × 48), with 32 vertical layers (up to an altitude ~120 km), a dynamical step of 1.5 min and a physical time step of 15 min. The water mass mixing ratio (mmr) obtained by the model at ~2.2 m was converted to H₂O partial pressure ($p_{\text{H}_2\text{O}}$) according to: $p_{\text{H}_2\text{O}} = 44/18 \times \text{mmr} \times p_{\text{surf}}$ and then converted to relative humidity RH at the surface: $\text{RH}_{\text{surf}} = p_{\text{H}_2\text{O}}/p_{\text{sat}}(T_{\text{surf}})$, where $p_{\text{sat}}(T_{\text{surf}})$ is the saturation vapor pressure of water ice calculated at the surface temperature. The total yearly duration that each grid cell spends in the appropriate RH– T_{surf} space was computed using 48 model outputs per day (30 min apart), 669 days/year, and by summing up all the time periods during which both the RH and T_{surf} variables remained within the limits of the space domain given by the equations in Supplementary Table 7. The precise timings of domain crossing were calculated by interpolating the RH and T_{surf} variables between each output. The time fraction of the year obtained at each grid point was mapped with a Robinson projection, using 15 contour levels (with IDL 8.5), on top of MOLA topographic contours.

Data availability

Rover Environmental Monitoring Station (REMS) data are available in the Planetary Data System (PDS) https://atmos.nmsu.edu/PDS/data/mslrem_1001/DATA. Underlying data for the main figures are included as Excel files in the source data. All data used for plotting the main figures and supplementary figures and those presented in Supplementary Tables are available at Science Data Bank⁷⁴, <https://doi.org/10.11922/sciencedb.00915>. The experimental operation, modeling equations, simulation code, visualization tools, and methodology-related discussions are all available as Supplementary Notes in the Supplementary Information.

Code availability

The ternary aqueous chemistry codes (C programs for deliquescence surface calculations; awk script for data formatting; gnuplot script for graph plotting) used in this study are available at Science Data Bank, <https://doi.org/10.11922/sciencedb.00911>. The softwares used in this study are accessible at following links provided. The awk: www.gnu.org/software/gawk/; the GCC compiler: gcc.gnu.org; the Dev-Cpp compiler: sourceforge.net/projects/orwelldevcpp. The Gnuplot: www.gnuplot.info. The ISLEC software and models can be accessed from a PHP based Web interface with a single point calculation mode (www.islec.net/islec-web/islec-web-mg-cl-clo4; www.islec.net/islec-web-ca-cl-clo4). The LMD General Circulation Model is available on request from the LMD team.

Received: 19 March 2021; Accepted: 12 January 2022;

Published online: 01 February 2022

References

- Chevrier, V. F., Hanley, J. & Altheide, T. S. Stability of perchlorate hydrates and their liquid solutions at the Phoenix landing site, Mars. *Geophys. Res. Lett.* **36**, L10202 (2009) <https://doi.org/10.1029/2009gl037497>.

- Toner, J. D. & Catling, D. C. Water activities of NaClO₄, Ca(ClO₄)₂, and Mg(ClO₄)₂ brines from experimental heat capacities: Water activity >0.6 below 200 K. *Geochim. Cosmochim. Ac.* **81**, 164–174 (2016).
- Toner, J. D. & Catling, D. C. Chlorate brines on Mars: implications for the occurrence of liquid water and deliquescence. *Earth Planet. Sci. Lett.* **497**, 161–168 (2018).
- Brundrett, M., Yan, W. L., Velazquez, M. C., Rao, B. & Jackson, W. A. Abiotic reduction of chlorate by Fe(II) minerals: implications for occurrence and transformation of oxy-chlorine species on Earth and Mars. *ACS Earth Space Chem.* **3**, 700–710 (2019).
- Mitra, K. & Catalano, J. G. Chlorate as a potential oxidant on Mars: rates and products of dissolved Fe(II) oxidation. *J. Geophys. Res. Planets* **124**, 2893–2916 (2019).
- Mitra, K., Moreland, E. L. & Catalano, J. G. Capacity of chlorate to oxidize ferrous iron: implications for iron oxide formation on Mars. *Minerals* **10**, 729 (2020).
- Lynch, K. L. et al. Evidence for biotic perchlorate reduction in naturally perchlorate-rich sediments of Pilot Valley Basin, Utah. *Astrobiology* **19**, 629–641 (2019).
- Wang, X. et al. Multiphase volatilization of halogens at the soil-atmosphere interface on Mars. *J. Geophys. Res. -Planets* **126**, e2021JE006929 (2021).
- Clark, J. et al. A review of sample analysis at Mars-Evolved Gas Analysis Laboratory analog work supporting the presence of perchlorates and chlorates in Gale Crater, Mars. *Minerals* **11**, 475 (2021).
- Hecht, M. H. et al. Detection of perchlorate and the soluble chemistry of Martian soil at the Phoenix Lander site. *Science* **325**, 64–67 (2009).
- Glavin, D. P. et al. Evidence for perchlorates and the origin of chlorinated hydrocarbons detected by SAM at the Rocknest aeolian deposit in Gale Crater. *J. Geophys. Res. -Planets* **118**, 1955–1973 (2013).
- Leshin, L. A. et al. Volatile, isotope, and organic analysis of Martian fines with the Mars Curiosity rover. *Science* **341**, 1238937 (2013).
- Ming, D. W. et al. Volatile and organic compositions of sedimentary rocks in Yellowknife Bay, Gale Crater, Mars. *Science* **343**, 1245267 (2014).
- Kounaves, S. P., Carrier, B. L., O’Neil, G. D., Stroble, S. T. & Claire, M. W. Evidence of Mars perchlorate, chlorate, and nitrate in Mars meteorite EETA79001: Implications for oxidants and organics. *Icarus* **229**, 206–213 (2014).
- Sutter, B. et al. Measurements of Oxychlorine species on Mars. *Int. J. Astrobiol.* **16**, 203–217 (2017).
- Jaramillo, E. A., Royle, S. H., Claire, M. W., Kounaves, S. P. & Sephton, M. A. Indigenous organic-oxidized fluid interactions in the Tissint Mars meteorite. *Geophys. Res. Lett.* **46**, 3090–3098 (2019).
- Jackson, W. A. et al. Global patterns and environmental controls of perchlorate and nitrate co-occurrence in arid and semi-arid environments. *Geochim. Cosmochim. Ac.* **164**, 502–522 (2015).
- Jackson, W. A. et al. Widespread occurrence of (per)chlorate in the Solar System. *Earth Planet. Sci. Lett.* **430**, 470–476 (2015).
- Navarro-Gonzalez, R., Vargas, E., de la Rosa, J., Raga, A. C. & McKay, C. P. Reanalysis of the Viking results suggests perchlorate and organics at midlatitudes on Mars. *J. Geophys. Res. -Planet* **115**, E12010 (2010).
- Clark, B. C. et al. Chemical composition of Martian fines. *J. Geophys. Res. -Solid Earth* **87**, 10059–10067 (1982).
- Jackson, W. A., Wang, S. X., Rao, B., Anderson, T. & Estrada, N. L. Heterogeneous production of perchlorate and chlorate by ozone oxidation of chloride: Implications on the source of (per)chlorate in the Solar System. *ACS Earth Space Chem.* **2**, 87–94 (2018).
- Schuttlefield, J. D., Sambur, J. B., Gelwicks, M., Eggleston, C. M. & Parkinson, B. A. Photooxidation of chloride by oxide minerals: implications for perchlorate on Mars. *J. Am. Chem. Soc.* **133**, 17521–17523 (2011).
- Wu, Z. C. et al. Forming perchlorates on Mars through plasma chemistry during dust events. *Earth Planet. Sci. Lett.* **504**, 94–105 (2018).
- Zhao, Y. Y. S., McLennan, S. M., Jackson, W. A. & Karunatillake, S. Photochemical controls on chlorine and bromine geochemistry at the Martian surface. *Earth Planet. Sci. Lett.* **497**, 102–112 (2018).
- Cull, S. C. et al. Concentrated perchlorate at the Mars Phoenix landing site: Evidence for thin film liquid water on Mars. *Geophys. Res. Lett.* **37**, L22203, (2010) <https://doi.org/10.1029/2010gl045269>.
- Gough, R. V., Chevrier, V. F. & Tolbert, M. A. Formation of aqueous solutions on Mars via deliquescence of chloride-perchlorate binary mixtures. *Earth Planet. Sci. Lett.* **393**, 73–82 (2014).
- Martin-Torres, F. J. et al. Transient liquid water and water activity at Gale crater on Mars. *Nat. Geosci.* **8**, 357–361 (2015).
- Kounaves, S. P. et al. Identification of the perchlorate parent salts at the Phoenix Mars landing site and possible implications. *Icarus* **232**, 226–231 (2014).
- Marion, G. M., Catling, D. C., Zahnle, K. J. & Claire, M. W. Modeling aqueous perchlorate chemistries with applications to Mars. *Icarus* **207**, 675–685 (2010).

30. Toner, J. D., Catling, D. C. & Light, B. Soluble salts at the Phoenix Lander site, Mars: a reanalysis of the wet chemistry laboratory data. *Geochim. Cosmochim. Ac.* **136**, 142–168 (2014).
31. Hogancamp, J. V. et al. Chlorate/Fe-bearing phase mixtures as a possible source of oxygen and chlorine detected by the sample analysis at Mars instrument in Gale Crater. *Mars. J. Geophys. Res. -Planets* **123**, 2920–2938 (2018).
32. Fischer, E., Martinez, G. M., Renno, N. O., Tamppari, L. K. & Zent, A. P. Relative humidity on Mars: new results from the Phoenix TECP sensor. *J. Geophys. Res. Planet.* **124**, 2780–2792 (2019).
33. Arvidson, R. E. Aqueous history of Mars as inferred from landed mission measurements of rocks, soils, and water ice. *J. Geophys. Res. Planet.* **121**, 1602–1626 (2016).
34. Savijärvi, H., McConnochie, T. H., Harri, A.-M. & Paton, M. Water vapor mixing ratios and air temperatures for three martian years from Curiosity. *Icarus* **326**, 170–175 (2019).
35. Stroble, S. T., McElhoney, K. M. & Kounaves, S. P. Comparison of the Phoenix Mars Lander WCL soil analyses with Antarctic Dry Valley soils, Mars meteorite EETA79001 sawdust, and a Mars simulant. *Icarus* **225**, 933–939 (2013).
36. Kounaves, S. P. et al. Discovery of natural perchlorate in the Antarctic Dry Valleys and its global implications. *Environ. Sci. Technol.* **44**, 2360–2364 (2010).
37. Hurowitz, J. A. et al. In situ and experimental evidence for acidic weathering of rocks and soils on Mars. *J. Geophys. Res.-Planet.* **111**, E02S19 (2006).
38. Tosca, N. J. & McLennan, S. M. Experimental constraints on the evaporation of partially oxidized acid-sulfate waters at the martian surface. *Geochim. Cosmochim. Ac.* **73**, 1205–1222 (2009).
39. Elsenousy, A., Hanley, J. & Chevrier, V. F. Effect of evaporation and freezing on the salt paragenesis and habitability of brines at the Phoenix landing site. *Earth Planet. Sci. Lett.* **421**, 39–46 (2015).
40. Toner, J. D., Catling, D. C. & Light, B. Modeling salt precipitation from brines on Mars: Evaporation versus freezing origin for soil salts. *Icarus* **250**, 451–461 (2015).
41. Smith, M. L., Claire, M. W., Catling, D. C. & Zahnle, K. J. The formation of sulfate, nitrate and perchlorate salts in the martian atmosphere. *Icarus* **231**, 51–64 (2014).
42. Stern, J. C. et al. Major volatiles evolved from eolian materials in Gale Crater. *Geophys. Res. Lett.* **45**, 240–210 (2018).
43. Arvidson, R. E. et al. Results from the Mars Phoenix lander robotic arm experiment. *J. Geophys. Res. Planet.* **114**, E00E02 (2009).
44. Pike, W. T. et al. Quantification of the dry history of the Martian soil inferred from in situ microscopy. *Geophys. Res. Lett.* **38**, L24201 (2011).
45. Smith, P. H. et al. H₂O at the Phoenix landing site. *Science* **325**, 58–61 (2009).
46. Goetz, W. et al. Microscopy analysis of soils at the Phoenix landing site, Mars: Classification of soil particles and description of their optical and magnetic properties. *J. Geophys. Res.-Planet.* **115**, E00e22 (2010) <https://doi.org/10.1029/2009je003437>.
47. Hollingsworth, J. L. et al. Orographic control of storm zones on Mars. *Nature* **380**, 413–416 (1996).
48. Wang, H. Cross-equatorial flushing dust storms and northern hemisphere transient eddies: An analysis for Mars Year 24. *J. Geophys. Res.-Planet.* **123**, 1732–1745 (2018).
49. Cantor, B. A., James, P. B., Caplinger, M. & Wolff, M. J. Martian dust storms: 1999 Mars Orbiter Camera observations. *J. Geophys. Res.-Planet.* **106**, 23653–23687 (2001).
50. Montabone, L., & Forget, F. *Forecasting dust storms on Mars: a short review*. In (eds. Levine, J. S., Winterhalter, D. & Kerschmann, R. L.) *Dust in the atmosphere of Mars and its impact on human exploration*. 132–151 (Cambridge Scholars Publishing, 2018).
51. Bertrand, T., Wilson, R. J., Kahre, M. A., Urata, R. & Kling, A. Simulation of the 2018 global dust storm on Mars using the NASA AMES Mars GCM: A multi-tracer approach. *J. Geophys. Res. Planet.* **125**, e2019JE006122 (2020).
52. Drube, L. et al. Magnetic and optical properties of airborne dust and settling rates of dust at the Phoenix landing site. *J. Geophys. Res.-Planet.* **115**, E00e23 (2010) <https://doi.org/10.1029/2009je003419>.
53. Sizemore, H. G. et al. In situ analysis of ice table depth variations in the vicinity of small rocks at the Phoenix landing site. *J. Geophys. Res.-Planet.* **115**, E00e09 (2010) <https://doi.org/10.1029/2009je003414>.
54. Mellon, M. T. et al. The periglacial landscape at the Phoenix landing site. *J. Geophys. Res.-Planet.* **114**, E00e06 (2009) <https://doi.org/10.1029/2009je003418>.
55. Knoll, A. H. & Grotzinger, J. Water on Mars and the prospect of Martian life. *Elements* **2**, 169–173 (2006).
56. Rivera-Valentín, E. G., Chevrier, V. F., Soto, A. & Martínez, G. Distribution and habitability of (meta)stable brines on present-day Mars. *Nat. Astron.* **4**, 756–761 (2020).
57. Hudson, T. L., Aharonson, O. & Schorghofer, N. Laboratory experiments and models of diffusive emplacement of ground ice on Mars. *J. Geophys. Res.-Planet.* **114**, E01002 (2009) <https://doi.org/10.1029/2008je003149>.
58. Röstel, L., Guo, J., Banjac, S., Wimmer-Schweingruber, R. F. & Heber, B. Subsurface radiation environment of Mars and its implication for shielding protection of future habitats. *J. Geophys. Res.-Planet.* **125**, e2019JE006246 (2020).
59. Schreinemakers, F. A. H. Graphische ableitungen aus den lösungs-isothermen eines doppelosalzes und seiner komponenten und mögliche formen der umwandlungskurve. *Zeitschrift für Physikalische Chemie* **11**, 81–109 (1893).
60. Li, D., Zeng, D., Yin, X., Gao, D. & Fan, Y. F. Phase diagrams and thermochemical modeling of salt lake brine systems. IV. Thermodynamic framework and program implementation for multicomponent systems. *Calphad* **71**, 101806 (2020).
61. Clegg, S. L., Pitzer, K. S. & Brimblecombe, P. Thermodynamics of multicomponent, miscible, ionic solutions. Mixtures including unsymmetrical electrolytes. *J. Phys. Chem.* **96**, 9470–9479 (1992).
62. Christov, C. Isopiestic determination of the osmotic coefficients of an aqueous MgCl₂ + CaCl₂ mixed solution at (25 and 50) °C. Chemical equilibrium model of solution behavior and solubility in the MgCl₂ + H₂O and MgCl₂ + CaCl₂ + H₂O systems to high concentration at (25 and 50) °C. *J. Chem. Eng. Data* **54**, 627–635 (2009).
63. Forget, F. et al. Improved general circulation models of the Martian atmosphere from the surface to above 80 km. *J. Geophys. Res.-Planet* **104**, 24155–24175 (1999).
64. Madeleine, J.-B., Forget, F., Millour, E., Montabone, L. & Wolff, M. J. Revisiting the radiative impact of dust on Mars using the LMD Global Climate Model. *J. Geophys. Res.-Planets* **116**, E11010 (2011).
65. Navarro, T. et al. Global Climate Modeling of the Martian water cycle with improved microphysics and radiatively active water ice clouds. *J. Geophys. Res.-Planets* **119**, 1479–1495 (2014).
66. Madeleine, J.-B., Forget, F., Millour, E., Navarro, T. & Spiga, A. The influence of radiatively active water ice clouds on the Martian climate. *Geophys. Res. Lett.* **39**, L23202 (2012).
67. Montmessin, F., Forget, F., Rannou, P., Cabane, M. & Haberle, R. M. Origin and role of water ice clouds in the Martian water cycle as inferred from a general circulation model. *J. Geophys. Res. Planets* **109**, E10004 (2004).
68. Pál, B., Kereszturi, Á., Forget, F. & Smith, M. D. Global seasonal variations of the near-surface relative humidity levels on present-day Mars. *Icarus* **333**, 481–495 (2019).
69. Colaitis, A. et al. A thermal plume model for the Martian convective boundary layer. *J. Geophys. Res. Planets* **118**, 1468–1487 (2013).
70. Smith, D. E. et al. The global topography of Mars and implications for surface evolution. *Science* **284**, 1495–1503 (1999).
71. Putzig, N. E. & Mellon, M. T. Apparent thermal inertia and the surface heterogeneity of Mars. *Icarus* **191**, 68–94 (2007).
72. Montabone, L. et al. Eight Martian years of dust climatology reconstructed from spacecraft observations, In *Proceedings of the Fifth International Workshop on the Mars Atmosphere: Modelling and Observation* (eds. Forget, F. & Millour, M.) 1404 (Oxford, U.K., 2014).
73. Montabone, L. et al. Martian year 34 column dust climatology from Mars climate sounder observations: reconstructed maps and model simulations. *J. Geophys. Res.-Planets*, e2019JE006111, (2020) <https://doi.org/10.1029/2019JE006111>.
74. Li, D. et al. Cryogenic perchlorate and chloride datasets (V2). Science Data Bank. (2021) <https://doi.org/10.1192/sciencedb.00915>.

Acknowledgements

We are very grateful to Scott McLennan for a constructive review, which greatly improved an earlier version of this paper. This work was supported by B-type Strategic Priority Program of the Chinese Academy of Sciences (No. XDB41000000), National Natural Science Foundation of China (No. 41703064, 41673072, 42173045, 41573056), Pre-research project on Civil Aerospace Technologies (No. D020102), Key Research Program of the Institute of Geology & Geophysics CAS (No. IGGCAS-201905), and West Light Foundation of CAS. Pierre-Yves Meslin acknowledges financial support from Centre National d'Etudes Spatiales (CNES).

Author contributions

Dongdong Li and Yu-Yan Sara Zhao designed the study and wrote the first draft of the manuscript. Dongdong Li conducted experiments and performed thermodynamic modeling. Pierre-Yves Meslin produced the global map of the ClO₄⁻/Cl⁻ fractionation region, using the latest version of the LMD GCM developed by Margaux Vals and François Forget. Zhongchen Wu helped to develop the conceptual model of ClO₄⁻/Cl⁻ fractionation related to aeolian processes on Mars. All authors contributed to editing and discussion of the paper.

Competing interests

The authors declare no competing interests.

Additional information

Supplementary information The online version contains supplementary material available at <https://doi.org/10.1038/s43247-022-00345-5>.

Correspondence and requests for materials should be addressed to Yu-Yan Sara Zhao.

Peer review information *Communications Earth & Environment* thanks the anonymous reviewers for their contribution to the peer review of this work. Primary Handling Editor: Joe Aslin.

Reprints and permission information is available at <http://www.nature.com/reprints>

Publisher's note Springer Nature remains neutral with regard to jurisdictional claims in published maps and institutional affiliations.



Open Access This article is licensed under a Creative Commons Attribution 4.0 International License, which permits use, sharing, adaptation, distribution and reproduction in any medium or format, as long as you give appropriate credit to the original author(s) and the source, provide a link to the Creative Commons license, and indicate if changes were made. The images or other third party material in this article are included in the article's Creative Commons license, unless indicated otherwise in a credit line to the material. If material is not included in the article's Creative Commons license and your intended use is not permitted by statutory regulation or exceeds the permitted use, you will need to obtain permission directly from the copyright holder. To view a copy of this license, visit <http://creativecommons.org/licenses/by/4.0/>.

© The Author(s) 2022